

FULL PAPER

Design of an underactuated anthropomorphic hand with mechanically implemented postural synergies

Kai Xu^{a*}, Huan Liu^a, Yuheng Du^a and Xiangyang Zhu^b

^aUM-SJTU Joint Institute, Shanghai Jiao Tong University, Shanghai, China; ^bSchool of Mechanical Engineering, Shanghai Jiao Tong University, Shanghai, China

(Received 7 April 2014; revised 5 July 2014; accepted 15 August 2014)

Neurology shows that human controls dozens of muscles for hand poses in a coordinated manner and such coordination is referred as to a postural synergy. The concept of postural synergies was recently adopted in the control of robotic hands. With the synergies implemented digitally in a controller, all the motors in an anthropomorphic robotic hand can be controlled via a few synergy inputs. Aiming at exploring alternative approaches for synergy realization, this paper proposes to implement the postural synergies using a mechanical transmission unit. Two rotation inputs can be scaled, combined, and mapped to the rotary outputs to drive an anthropomorphic hand, enabling not only various grasping tasks but also a manipulation motion. Synergy synthesis and design of the anthropomorphic hand are firstly presented. The transmission unit as the implementation of the postural synergies is then elaborated. Tests were performed to quantify how well the synergies could be reproduced via this transmission unit. The results suggest it might be promising to construct a low cost yet versatile prosthetic hand by implementing the postural synergies mechanically.

Keywords: anthropomorphic hand; robotic hand; underactuation; postural synergy; planetary gear

1. Introduction

It is a challenging task to construct an anthropomorphic prosthetic hand that can reproduce the delicate motions of the biological original. An ideal prosthetic hand is expected to be versatile for various daily tasks and controllable through a biosignal interface, such as electromyography or electroencephalography. However, limited bandwidth of these interfaces used to prevent fully actuated robotic hands from being applied as prostheses if each joint needs individual control to perform grasping tasks, even though many designs were absolutely the state-of-the-art (e.g. the ones in [1–4]).

Many prosthetic hands hence followed an underactuated design approach. Researchers often refer to grasp taxonomy in order to assure the prosthetic hand motions are functional enough for various daily tasks. Study on the grasp taxonomy can be traced back to the 1950s [5] with milestones marked in the 1980s.[6,7] The taxonomy of discrete hand postures was shown useful by the development of several prosthetic hands [8–11] and it was still being expanded by recent results.[12,13] However, in the design of underactuated prosthetic hands, referring to the discrete grasp taxonomy does not directly indicate how to assign actuation and coupling relations among the hand joints. Alternative approaches might be needed to better guide the development of underactuated prosthetic hands.

Findings in neurology suggested a possible way of achieving dexterous control of a multi-Degree of Freedom robotic hand via a few inputs. It was showed that Central Nervous System (CNS) controls dozens of muscles for hand poses in a coordinated manner. Such coordination is referred as to a postural synergy, which corresponds to the coupled flexion and/or extension actuation statuses of the involved muscles.[14] CNS combines postural synergies, adjusting each synergy's coefficient (weight), to realize various hand motions. Combination of two primary postural synergies accounts for about 84% of the variance of many grasping postures.[15] What's more, CNS switches between different sets of postural synergies for distinct grasping and manipulations tasks.[16]

Adoption of these findings allowed a fully actuated robotic hand to be applied as prosthesis. Two biosignal channels as synergy inputs would act as the coefficients while combining two postural synergies in the controller. Several designs have demonstrated this idea, such as the DLR II Hand,[17] the SAH hand,[18] the UB hand,[19] and the ACT hand [20,21] with two to three synergies for the control of 12–24 actuators. Although this approach seems straightforward, there are still concerns regarding the system cost, reliability, battery life, and so on stemmed from the use of multiple sets of miniature servomotors with amplifiers, sensors, and controllers. It

*Corresponding author. Email: k.xu@sjtu.edu.cn

might still be necessary to explore alternative possibilities to implement postural synergies.

It is possible to implement postural synergies mechanically, demonstrated by Brown and Asada using differential pulleys.[22] Although various postures of the hand were formed using two synergy inputs, this approach has limited potential due to the difficulty of arranging the complicated pulley system in a more practical configuration. This paper hence proposes to realize the mechanical implementation of the postural synergies in an underactuated anthropomorphic hand using planetary gears, as shown in Figure 1. It would be explained later in this paper that this approach could be more practically meaningful. With the feasibility demonstrated in this paper and a further miniaturized gear system, it is promising to improve the design into a form more suitable for prosthetic use.

Besides proposing to implement postural synergies using planetary gears, the contributions of this paper also include the attempt of realizing a manipulation task using only two synergy inputs. This upgrade in a prosthetic hand's motion capability from grasping to manipulation was inspired by the milestone work done by Ciocarlie and Allen [23], where poses of different hands could be optimized to form various grasps. Two synergy inputs can be adjusted to grasp distinct objects; they might also be used to manipulate the same object, since manipulation of one object is essentially a smooth transition between different grasping patterns of the same object.

The paper is organized as follows. Section 2 presents the postural synergy synthesis where synergy components were obtained, refined, and experimentally adjusted for specific postures. Section 3 presents the design of the anthropomorphic hand with the experimentation reported in Section 4. Conclusions are presented in Section 5.

2. Postural synergy synthesis

This paper attempts to present a complete process of designing an underactuated anthropomorphic hand for a

manipulation task and grasps. The proposed manipulation paradigm is to rotate two rehabilitation training balls on palm using coordinated finger motions as shown in Figures 1 and 2. This exercise helps the elderly or patients after mild stroke to maintain or recover their hand motor functions. Although this motion sequence might not seem practically useful for amputees, the motivation here is to demonstrate the effectiveness of this presented design process. Although this manipulation task is shown successful later in this paper, it should be noted that the manipulation of arbitrary objects is not guaranteed due to the specific synergies synthesized from this particular motion sequence.

Postural synergies are usually extracted as the first two principal components from recorded joint angles of a hand under various poses. Then the two synergies could be combined to map two synergy inputs to the hand joint angles. When grasping tasks were performed, the synergy inputs were adjusted to properly form grasping poses. These adjustments essentially compensated for (i) the discrepancy between the original postural synergies and their implementations and (ii) the neglected higher order synergies. When manipulation tasks are intended, the synergy inputs will be primarily used to transform the hand from one pose to another in a continuous manner, limiting their roles in compensating/correcting the implemented postural synergies. Hence, synergy discrepancy should be minimized for the hand design to satisfactorily reproduce the specific motion sequence using only two synergy inputs.

In order to minimize the synergy discrepancy, this paper introduces a cheap and effective technique by constructing a dummy hand for the synthesis of postural synergies. Instead of inviting 5–10 human subjects, asking them to manipulate the rehabilitation training balls, recording and analyzing the human hand motions using sophisticated systems such as CyberGloveTM or ViconTM cameras, this dummy hand was built and manually posed to manipulate the training balls as in Figure 2. Joint

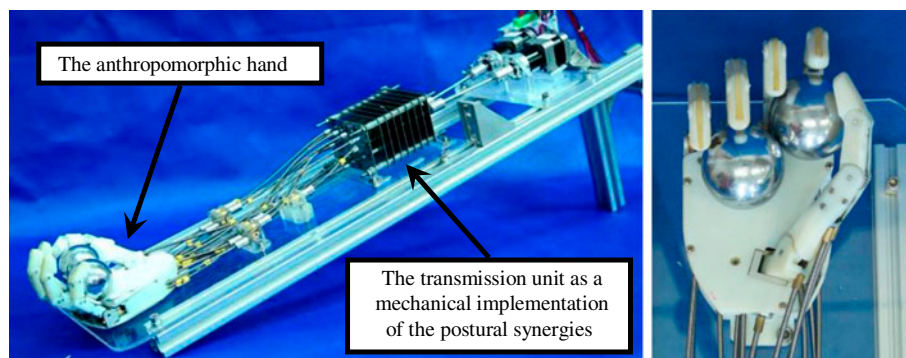


Figure 1. An anthropomorphic robotic hand actuated by two motors through a transmission unit while manipulating two rehabilitation training balls.

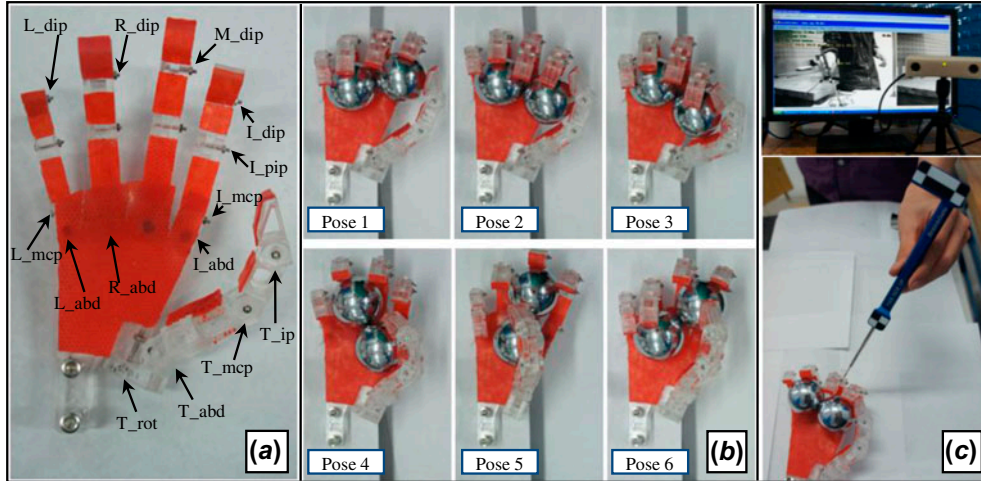


Figure 2. (a) A dummy hand was constructed; (b) and manually posed for a motion sequence of manipulating two rehabilitation training balls; (c) joint angles of the dummy hand were measured using an optical tracker.

angles of the dummy hand under each pose were measured and directly used for the synergy synthesis. This approach avoids the challenges studied in [24], which minimizes synergy discrepancies while mapping the kinematics from a human hand to a robotic hand.

2.1. Original postures and raw synergies

All the joints in the anthropomorphic dummy hand as in Figure 2(a) are passive with friction big enough to maintain a hand pose against external disturbance (e.g. gravity). The arrangements of revolute joints provided motion capabilities as consistent as possible to a human hand but also left enough space to realize actuations of these joints. The dummy hand had identical enveloping dimensions and geometry as the one constructed with transmissions and actuations in Figure 6.

The dummy hand was manually posed for six key poses as shown in Figure 2(b). The choices of the six key poses were based on the observation how a human subject manipulates such rehabilitation training balls. Since the experiment of manipulating these two balls in Section 4.3 was successful, six key poses seem enough. Joints of this dummy hand are indicated in Figure 2(a) with their angle values and motion ranges summarized in Table 1. The joints are named as follows. Letters *T*, *I*, *M*, *R*, and *L* before the underscore indicate the joints for the thumb, the index, the middle, the ring, and the little fingers, respectively. Abbreviations of *rot*, *mcp*, *ip*, *abd*, *pip*, and *dip* after the underscore indicate the rotation, the metacarpophalangeal, the interphalangeal, the abduction, the proximal, and the distal interphalangeal joints, respectively. For all the interphalangeal joints and the metacarpophalangeal joints, zero values are defined as

they reach their full extensions whereas positive values are defined for flexion motions. For all the abduction joints, positive values are defined in their abduction motions. Abduction joint of the middle finger is fixed, since abduction motions are measured relatively. Positive value of the thumb rotation joint is defined in its opposition motion. In total, there are 19 joints in the dummy hand (the middle finger does not possess an abduction joint). This corresponds to the 19 rows in Table 1.

In each pose, joint angles were measured using an optical tracker (Micron Tracker SX60 from Claron Technology Inc.) as in Figure 2(c). Two adjacent intersecting surfaces of the two adjacent phalanges were first characterized by obtaining coordinates of three points on the surfaces in the tracker frame. The joint angle was then obtained from the dot product of the two surface normals.

Each pose in Figure 2(b) corresponds to a pose vector \mathbf{j}_i ($i = 1, 2, \dots, 6$), which consists of all the joint angles. The index i indicates the poses and the corresponding synergy inputs (as explained later, each pose corresponds to two synergy inputs). According to Table 1, it could be noticed that motions of the four distal interphalangeal joints (I_{dip} , M_{dip} , R_{dip} , and L_{dip}) were approximately equally coupled to the motions of the four proximal interphalangeal joints (I_{pip} , M_{pip} , R_{pip} , and L_{pip}). Hence, dimension of the pose vector can be reduced to 15, namely, $\mathbf{j}_i \in \mathbb{R}_{15 \times 1}$, whereas the coupling between the *dip* joints and the *pip* joints is approximated as follows:

$$\begin{aligned} j_{I_{dip}} &= j_{I_{pip}} & j_{M_{dip}} &= j_{M_{pip}} & j_{R_{dip}} &= j_{R_{pip}} \\ j_{L_{dip}} &= j_{L_{pip}} \end{aligned} \quad (1)$$

Table 1. Joint ranges and joint angles of the dummy hand in the key poses in Figure 2.

Joints	Joint ranges (°)	Joint angles (°) of poses in Figure 2(b)					
		Pos 1	Pos 2	Pos 3	Pos 4	Pos 5	Pos 6
T_{rot}	[0, 135]	48	44	37	65	87	69
T_{mcp}	[0, 90]	24	36	42	45	50	35
T_{ip}	[0, 90]	29	40	50	50	55	40
T_{abd}	[0, 80]	30	38	43	52	55	40
I_{mcp}	[0, 90]	45	58	75	50	25	16
M_{mcp}	[0, 90]	55	43	45	1	4	21
R_{mcp}	[0, 90]	55	50	41	0	17	52
L_{mcp}	[0, 90]	55	50	73	50	55	55
I_{pip}	[0, 100]	59	54	52	55	53	56
M_{pip}	[0, 100]	63	85	69	77	69	69
R_{pip}	[0, 100]	75	69	70	72	73	76
L_{pip}	[0, 100]	71	65	57	80	69	78
I_{abd}	[0, 20]	5	10	10	5	5	17
R_{abd}	[0, 20]	5	10	8	13	10	12
L_{abd}	[0, 20]	15	19	10	16	15	18
I_{dip}	[0, 90]	58	53	52	55	53	56
M_{dip}	[0, 90]	60	81	66	75	66	60
R_{dip}	[0, 90]	72	68	66	72	70	72
L_{dip}	[0, 90]	69	60	52	70	66	70

The six pose vectors from Figure 2(b) can be put side to side to form a pose matrix \mathbf{J} whose numerical values are from the T_{rot} row to the L_{abd} row in Table 1:

$$\mathbf{J}_{15 \times 6} = [\mathbf{j}_1 \quad \mathbf{j}_2 \quad \cdots \quad \mathbf{j}_6] \quad (2)$$

Although each pose involves the rotations of 15 hand joints, postural synergies could be extracted to reduce the dimension of the joint space. If only two synergy inputs are expected, an ideal scenario is that all \mathbf{j}_i can be linearly spanned using two basis vectors. In order to examine how close the actual matrix \mathbf{J} is to the ideal case, Singular Value Decomposition (SVD) was introduced:

$$\begin{aligned} \mathbf{J} &= \bar{\mathbf{J}} + \mathbf{U}_{15 \times 15} \Sigma_{15 \times 6} \mathbf{V}_{6 \times 6}^T \\ &= \bar{\mathbf{J}} + [\mathbf{u}_1 \quad \mathbf{u}_2 \quad \cdots \quad \mathbf{u}_{15}] \\ &\quad \cdot \begin{bmatrix} \text{diag}(\delta_1, \delta_2, \cdots, \delta_6) \\ \mathbf{0}_{9 \times 6} \end{bmatrix} \begin{bmatrix} \mathbf{v}_1^T \\ \mathbf{v}_2^T \\ \vdots \\ \mathbf{v}_6^T \end{bmatrix} \end{aligned} \quad (3)$$

where $\bar{\mathbf{J}} = [\bar{\mathbf{j}}_1 \quad \bar{\mathbf{j}}_2 \quad \bar{\mathbf{j}}_3 \quad \bar{\mathbf{j}}_4 \quad \bar{\mathbf{j}}_5 \quad \bar{\mathbf{j}}_6]$ is the average pose matrix, $\bar{\mathbf{j}}_k = \frac{1}{6} \sum_{i=1}^6 \mathbf{j}_i$ and $\mathbf{v}_k^T \in \mathfrak{R}_{1 \times 6}$.

The biggest two singular values are 85.91 and 55.51, whereas the third biggest singular value is 26.25. The ratio of the sum of the first two singular values and the sum of all the singular values is 0.70. Since the biggest two singular values are considerably bigger than the rest, the singular values δ_k ($k = 3, 4, 5, 6$) are neglected. Then the pose matrix \mathbf{J} can be approximated by an approximate

pose matrix $\tilde{\mathbf{J}}$ as in Equation (4) so that each hand pose can be approximated as in Equation (5):

$$\begin{aligned} \tilde{\mathbf{J}} &= \bar{\mathbf{J}} + [\mathbf{u}_1 \quad \mathbf{u}_2] \begin{bmatrix} \delta_1 \mathbf{v}_1^T \\ \delta_2 \mathbf{v}_2^T \end{bmatrix} \\ &= \bar{\mathbf{J}} + [\mathbf{u}_1 \quad \mathbf{u}_2] \begin{bmatrix} q_{11} & q_{12} & \cdots & q_{16} \\ q_{21} & q_{22} & \cdots & q_{26} \end{bmatrix} \end{aligned} \quad (4)$$

$$\tilde{\mathbf{j}}_i = \bar{\mathbf{j}} + q_{1i} \mathbf{u}_1 + q_{2i} \mathbf{u}_2, i = 1, 2, \dots, 6 \quad (5)$$

Vectors \mathbf{u}_1 and \mathbf{u}_2 are referred to as the postural synergies. With q_{1i} and q_{2i} as synergy inputs, various hand poses could be formed while linearly combining the two postural synergies.

A pose error matrix \mathbf{J}_{err} can then be defined as:

$$\mathbf{J}_{err} = \mathbf{J} - \tilde{\mathbf{J}} \quad (6)$$

This pose error matrix \mathbf{J}_{err} is visualized in Figure 3, where X and Y axes stand for joints and poses (e.g. there are 15 joints in one pose) with Z axis standing for the errors in the joints under different poses. The biggest error is about 12.8° and the norm of these errors is 26.26° .

2.2. Adjusted poses and postural synergies

In the task of rotating two rehabilitation training balls on the palm, the errors from Equation (6) are not of equal importance. Some errors corresponded to fingers that touched neither of the balls. After checking the significance of each individual error in Figure 3, two critical errors were identified:

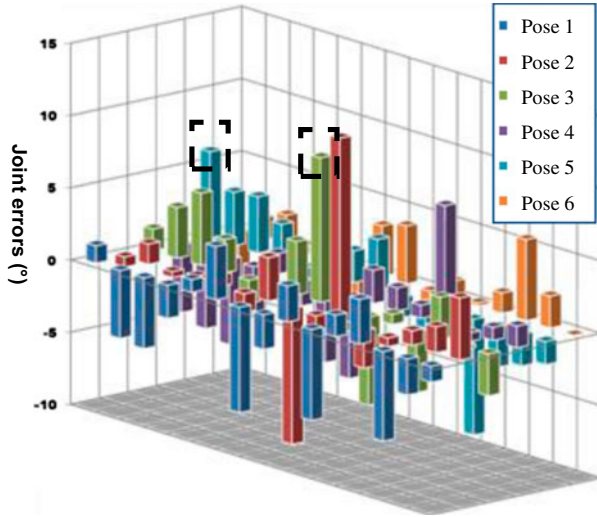


Figure 3. Visualization of the pose error matrix with critical errors marked.

- One error belongs to the L_mcp joint of Pose 3 from Figure 2(b). Numerical value of this error is $+10^\circ$. According to the definition of the errors in Equation (6), an error of $+10^\circ$ means this joint rotated 10° less. Referring to Figure 2(b), this error is critical because the little finger will not be able to push the left-upper ball toward the right side, if the L_mcp joint rotates less than the desired value.
- The other critical error belongs to the T_rot joint of Pose 5 from Figure 2(b). Numerical value of this error is $+6^\circ$, meaning this joint rotated 6° less. Referring to Pose 4 and Pose 5 in Figure 2(b), this error is critical because the thumb will not be able to push the right-lower ball toward the left side, if the T_rot joint does not rotate enough.

In order to reduce the critical errors of the L_mcp and the T_rot joints under the corresponding poses, the original joint values of these two joints were adjusted until the two critical errors were reduced to below 1° . The resulting adjustments are as follows. The L_mcp joint angle of Pose 3 in Figure 2(b) was increased from 73° to 85° , whereas the T_rot joint angle of Pose 5 in Figure 2(b) was increased from 87° to 95° . These two angles are in italic font in Table 1. The procedure from Equation (3) to Equation (6) was repeated to obtain the updated values of \mathbf{J} , $\bar{\mathbf{J}}$, $\bar{\mathbf{J}}$, \mathbf{u}_k , q_{ki} ($k = 1, 2, i = 1, 2, \dots, 6$), and \mathbf{J}_{err} . The new \mathbf{J}_{err} matrix was visualized as in Figure 4.

Figure 4 shows clearly that the critical errors were suppressed, even though the error with the biggest absolute value rose to 13.2° with the norm of these errors at 27.01° . The updated \mathbf{J} , \mathbf{u}_k , and q_{ki} ($k = 1, 2,$

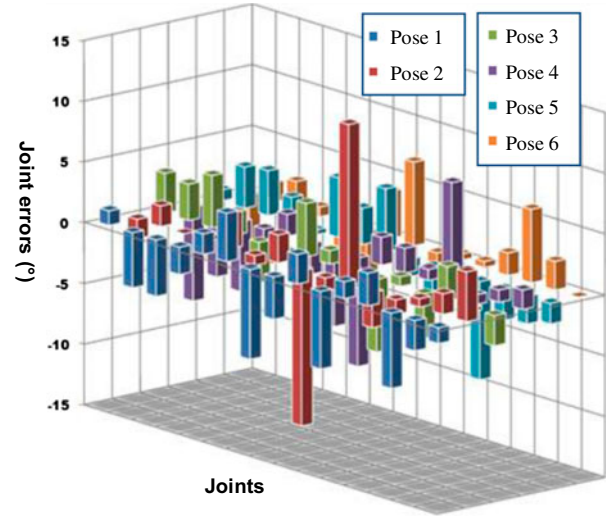


Figure 4. Visualization of the updated pose error matrix.

$i = 1, 2, \dots, 6$) are summarized in Table 2 with the relation among them as in Equation (5).

The pose adjustment process suggests that it is not necessary to always strictly stick to the measured poses as far as the regenerated poses better approximate the measured ones. It should be noted that the identification of the two critical errors does not possess a universal sense, which means that these two errors were spotted

Table 2. The average pose, the postural synergies, and the synergy inputs for the adjusted poses.

Joints	Average pose $\bar{\mathbf{j}}$ ($^\circ$)	Postural synergies			
		\mathbf{u}_1	\mathbf{u}_2		
<i>T_rot</i>	59.7	-0.49	0.24		
<i>T_mcp</i>	38.7	-0.16	-0.21		
<i>T_ip</i>	44.0	-0.15	-0.23		
<i>T_abd</i>	43.0	-0.20	-0.17		
<i>I_mcp</i>	44.8	0.34	-0.66		
<i>M_mcp</i>	28.2	0.56	0.12		
<i>R_mcp</i>	35.8	0.44	0.50		
<i>L_mcp</i>	58.3	0.15	-0.25		
<i>I_pip</i>	54.8	0.01	0.06		
<i>M_pip</i>	72.0	-0.01	-0.11		
<i>R_pip</i>	72.5	-0.02	0.08		
<i>L_pip</i>	70.0	-0.13	0.14		
<i>I_abd</i>	8.7	0.03	0.08		
<i>R_abd</i>	9.7	-0.05	-0.02		
<i>L_abd</i>	15.5	-0.02	0.07		
Pose 1 inputs ($^\circ$)		Pose 2 inputs ($^\circ$)	Pose 3 inputs ($^\circ$)		
q_{11}	36.2	q_{12}	28.1	q_{13}	37.6
q_{21}	21.0	q_{22}	-1.1	q_{23}	-31.5
Pose 4 inputs ($^\circ$)		Pose 5 inputs ($^\circ$)	Pose 6 inputs ($^\circ$)		
q'_{14}	-38.5	q'_{15}	-52.4	q'_{16}	-11.0
q_{24}	-25.1	q_{25}	2.6	q_{26}	34.1

by manually estimating the possibilities of all the errors whether they would hinder the manipulation task. If the elements in the pose matrix are arbitrarily adjusted, some errors might newly become critical. For this reason, if this adjustment is formulated as an optimization, it would be inappropriate to only minimize these two particular errors. However, it could be challenging to identify all the errors whether they are critical and dynamically update the cost function. A direct approach was hence adopted here and it was manually confirmed that the remaining errors in \mathbf{J}_{err} are less likely to affect the manipulation task. The experiment presented in Section 4.3 supports the estimation.

Equation (5) indicates that the two synergy inputs q_1 and q_2 could be used to actuate the hand from the average pose $\bar{\mathbf{j}}$ to an arbitrary hand pose. With the synergies \mathbf{u}_1 and \mathbf{u}_2 from Table 2 and the joint ranges from Table 1, a valid actuation zone for the synergy inputs q_1 and q_2 is visualized in Figure 5.

3. Hand design descriptions

This paper proposes to implement the postural synergies mechanically. Two synergy inputs q_1 and q_2 shall be combined, scaled, and mapped to the outputs through a transmission to drive the anthropomorphic hand from its average pose $\bar{\mathbf{j}}$, according to Equation (5). The transmission unit is hence referred as to the mechanical implementation of the postural synergies. The use of two postural synergies results from the fact that the biggest two singular values from Equation (3) are considerably bigger than the rest. Besides this fact, it is also extremely challenging to design a mechanical transmission unit which could combine three or more postural synergies.

Such a mechanical synergy implementation was firstly attempted by Brown and Asada using differential pulleys.[22] The complexity of the pulley system and the

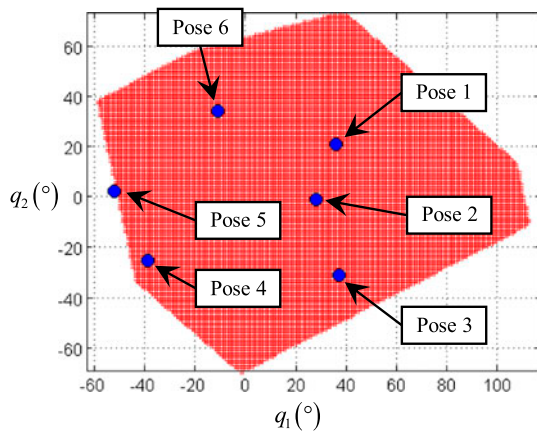


Figure 5. Valid actuation zone for the two synergy inputs q_1 and q_2 .

requirement of maintaining the cable tension diminished the potential for a practical use. This paper hence alternatively proposes to use planetary gears to realize the mechanical implementation of the postural synergies. As shown in Figure 6, the transmission and the actuators could be arranged in the forearm, whereas flexible shafts were used to connect the outputs from the transmission to drive the finger joints. A particular advantage of using the flexible shafts is that their rotations would be barely affected by a possible presence of wrist motions. On the contrary, even if the differential pulley system could be arranged in the forearm, cable routing would be quite challenging with the presence of a wrist. Furthermore, the planetary gear system could potentially offer better transmission accuracy than the pulley system.

Since the dummy hand was posed for the desired motion sequence of manipulating two training balls, kinematic features (e.g. arrangements of the joint axes) and enveloping dimensions of this anthropomorphic hand shall remain identical to the dummy hand.

The first version of the anthropomorphic hand design shown in Figure 6(a) was presented in [25]. Gear trains were used to realize the actuation of the interphalangeal joints. This version was abandoned due to the bulky appearance and the flimsy construction resulted from the excessive backlashes of the multi-stage gear trains. A second version was then designed and constructed as shown in Figure 6(b). The rest of this section elaborates the new anthropomorphic hand design and the planetary gear-based transmission unit as the mechanical implementation of the postural synergies.

3.1. Design descriptions of the hand

There are 19 joints in the dummy hand as indicated by the 19 rows in Table 1. These joints shall be actuated by

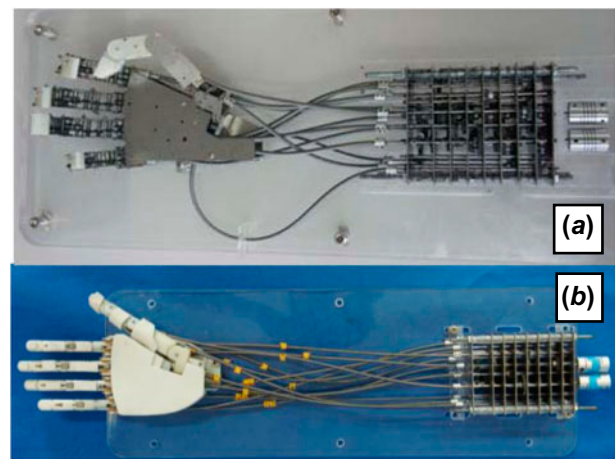


Figure 6. Design overview of the anthropomorphic hand and the mechanical synergy implementation: (a) first version and (b) second version.

properly arranged components. As mentioned above, flexible shafts were used to transmit rotary outputs to drive the hand joints. The main design features of the anthropomorphic hand hence lie on the realization of the transmission and actuation of the fingers using these rotations of the flexible shafts.

The actuation scheme of the thumb is shown in Figure 7. A flexible shaft was connected to a planetary gearhead (with a gear ratio of $945:52 \approx 18.17:1$) to drive the T_{rot} joint. Another flexible shaft was connected to a worm to drive a worm gear so as to drive the T_{abd} joint. The kinematic relations are shown in Equations (7) and (8) where $j_{T_{rot}}$ and $j_{T_{abd}}$ refer to the T_{rot} and the T_{abd} joint angles; $p_{T_{rot}}$ and $p_{T_{abd}}$ refer to the rotation angles of the flexible shafts for the T_{rot} and the T_{abd} joints. This naming convention also applies to Equation (9) to Equation (15). The worm has one start and the worm gear has 20 teeth. Other worms and worm gears used here possess the same specifications.

$$j_{T_{rot}} = p_{T_{rot}}/18.17 \tag{7}$$

$$j_{T_{abd}} = p_{T_{abd}}/20 \tag{8}$$

Two more flexible shafts were connected to two pairs of worms & gears to drive the T_{mcp} and the T_{ip} joints through two identical trains of spur gears and a coupler. In the gear train, the gear (Gear 3) has 28 teeth whereas the pinion (Gear 1) has 18 teeth with a module of 0.5. An idler gear was added to keep the rotations of Gear 1 and Gear 3 in the same direction. Gear 1 was attached to the worm gear and Gear 3 is attached to the thumb's proximal phalanx to drive the T_{mcp} joint or to a coupler to drive the T_{ip} joint. The dual arrangement of the worm gears for the T_{mcp} and the T_{ip} joints introduced coupling motions between them. Once the worm gear for the T_{mcp} joint was actuated, the worm gear for the T_{ip} joint should be actuated for the same amount in order to keep the T_{ip} joint unchanged. This coupling is reflected in Equation (10) and it will be accommodated in the transmission unit design.

$$j_{T_{mcp}} = p_{T_{mcp}}/20 \times 18/28 = 9p_{T_{mcp}}/280 \tag{9}$$

$$j_{T_{ip}} = 9(p_{T_{ip}} - p_{T_{mcp}})/280 = 9p_{T_{ip}}/280 - j_{T_{mcp}} \tag{10}$$

The actuation scheme of the fingers is shown in Figures 8 and 9. Since the actuation of the index, the middle, the ring, and the little fingers is similar, Figure 8 mainly shows the structure of the middle finger. Two flexible shafts were connected to two pairs of worms & gears. Worm Gear 1 was attached to the proximal phalanx so as to drive the M_{mcp} joint, as reflected in Equation (11). Worm Gear 2 was attached to Coupler 1 so that motion of the M_{mcp} joint is coupled to the M_{pip} joint. Coupler 2 connected the proximal phalanx and the distal phalanx so that the M_{pip} joint is also coupled to the M_{dip} joint. Similar designs could be

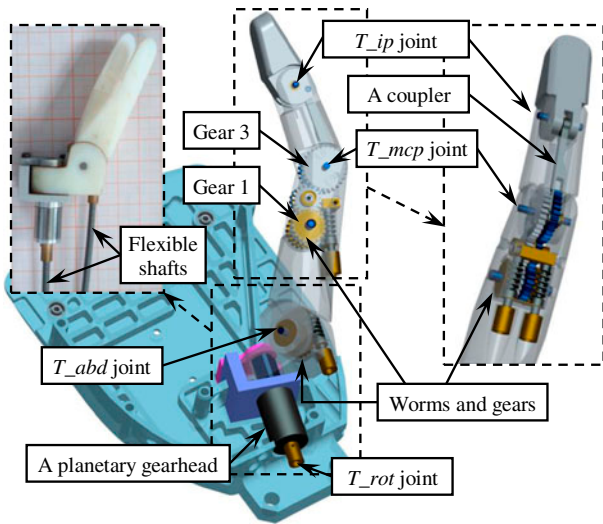


Figure 7. Actuation scheme of the thumb.

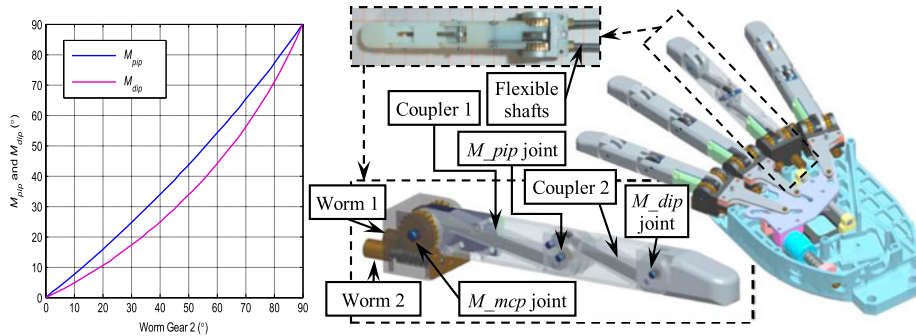


Figure 8. Actuation scheme of the metacarpophalangeal and interphalangeal joints.

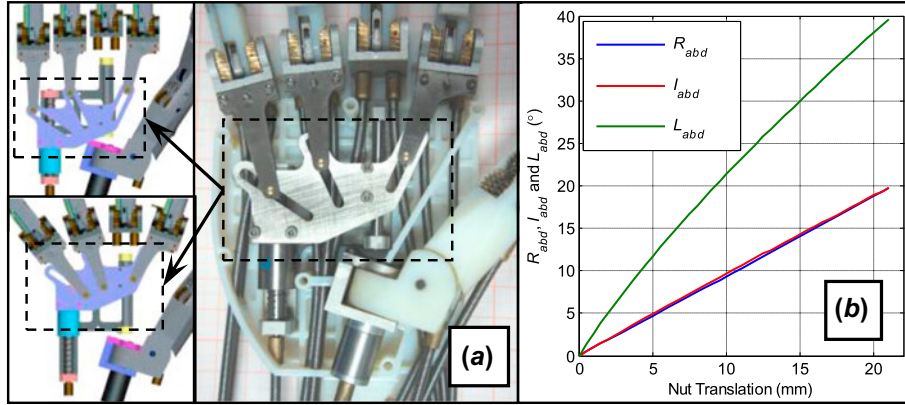


Figure 9. Actuation scheme of the fingers: (a) adduction and abduction motions and (b) motion trajectories.

found in [26,27]. The M_{pip} and the M_{dip} joint angles are plotted with respect to the rotation of Worm Gear 2 as in Figure 8 via a motion analysis performed in ProEngineer. It can be seen that the coupling between the Worm Gear 2 rotation and the M_{pip} joint is close to 1:1. Similar to the thumb design, the dual arrangement of the worm gears for the M_{mcp} and the M_{pip} joints also introduced coupling motions. Once the worm gear for the M_{mcp} joint was actuated, the worm gear for the M_{pip} joint should be actuated for the same amount in order to keep the M_{pip} joint unchanged. This coupling effect will be accommodated in the design of the transmission unit and the M_{pip} joint is actuated as in Equation (12).

$$\begin{aligned} \dot{j}_{M_{mcp}} &= p_{M_{mcp}}/20 & \dot{j}_{I_{mcp}} &= p_{I_{mcp}}/20 \\ \dot{j}_{R_{mcp}} &= p_{R_{mcp}}/20 & \dot{j}_{L_{mcp}} &= p_{L_{mcp}}/20 \end{aligned} \quad (11)$$

$$\begin{aligned} \dot{j}_{M_{pip}} &\approx (p_{M_{pip}} - p_{M_{mcp}})/20 \\ \dot{j}_{I_{pip}} &\approx (p_{I_{pip}} - p_{I_{mcp}})/20 \\ \dot{j}_{R_{pip}} &\approx (p_{R_{pip}} - p_{R_{mcp}})/20 \\ \dot{j}_{L_{pip}} &\approx (p_{L_{pip}} - p_{L_{mcp}})/20 \end{aligned} \quad (12)$$

According to Equation (5) and Table 2, abduction motions of the index, the ring, and the little fingers were also subjected to inputs q_1 and q_2 . This means three sets of transmission mechanisms would be needed. However, their synergies values (the rows for I_{abd} , R_{abd} , and L_{abd} in Table 2) are quite small, because they did not rotate much. In order to ease the design of the transmission unit, abduction motions of the three fingers were made coupled. As shown in Figure 9, a plate cam is actuated by a miniature ball screw with a lead of 2 mm. Translation of the plate cam introduces the coupled abduction motions of the three fingers. The motion axes of the abduction joints intersect with the motion axes of the mcp joints of the index, the ring, and the little

fingers. A motion analysis was again performed in Pro-Engineer. The I_{abd} , R_{abd} , and L_{abd} joint angles were plotted in Figure 9(b) with respect to the nut translation of the ball screw. The abduction motions are hence functions of the rotatory input p_{abd} of the flexible shaft as in Equation (13) to Equation (15).

$$\dot{j}_{I_{abd}} \approx 0.00556 p_{abd} \quad (13)$$

$$\dot{j}_{R_{abd}} \approx 0.00556 p_{abd} \quad (14)$$

$$\dot{j}_{L_{abd}} \approx 0.0111 p_{abd} \quad (15)$$

If all the hand joints could be actuated independently, the hand might better reproduce the poses formed by the dummy hand. In order to avoid over-complicating the design of the transmission unit, several joints in the hand were made coupled. In total, 13 outputs from the transmission unit, instead of 19 outputs, are now needed to drive the anthropomorphic hand.

3.2. The transmission unit as the mechanical synergy implementation

Due to the coupling (i) between the four dip joints and the respective pip joints, and the coupling (ii) of the abd joints, 13 synergy outputs would be needed to drive this underactuated hand. All the synergy outputs will be connected to the corresponding components (11 worms, one ball screw, and one planetary gearhead) using flexible shafts.

The transmission unit as the mechanically implemented postural synergies then shall linearly combines two synergy inputs (q_1 and q_2) to generate 13 synergy outputs ($p_{T_{rot}}$, $p_{T_{abd}}$, $p_{T_{mcp}}$, and so on) to drive the 19 joints of the prosthetic hands ($j_{T_{rot}}$, $j_{T_{abd}}$, $j_{T_{mcp}}$, and so on).

Implementing the postural synergy mechanically is to design a transmission unit so that each output is a linear combination of the inputs. The proposed approach using planetary gears could be seen from Figure 10. Two inputs q_1 and q_2 were shared by multiple sets of planetary gears in the following four configurations:

- Configuration A: q_1 is connected to the sun gear and q_2 is meshed with the ring gear (annulus); the carrier is the output.
- Configuration B: q_1 is connected to the sun gear and q_2 is meshed with the carrier; the ring gear is the output.
- Configuration C: q_1 is meshed with the ring gear and q_2 is connected to the sun gear; the carrier is the output.
- Configuration D: q_1 is meshed with the carrier and q_2 is connected to the sun gear; the ring gear is the output.

The outputs (p_A , p_B , p_C , and p_D) are now functions of the inputs q_1 and q_2 as in Equation (16) to Equation (19), where z_1 to z_4 are labeled in Figure 10; z_r and z_s are the teeth numbers of the ring gear and the sun gear, respectively. The outputs would be connected to the flexible shafts to drive the anthropomorphic hand.

$$p_A = \left(-\frac{z_3}{z_4}\right) \frac{z_s}{z_s + z_r} q_1 + \left(-\frac{z_3}{z_4}\right) \frac{z_r}{z_s + z_r} \left(-\frac{z_1}{z_2}\right) q_2 \quad (16)$$

$$p_B = \left(-\frac{z_3}{z_4}\right) \left(-\frac{z_s}{z_r}\right) q_1 + \left(-\frac{z_3}{z_4}\right) \frac{z_s + z_r}{z_r} \left(-\frac{z_1}{z_2}\right) q_2 \quad (17)$$

$$p_C = \left(-\frac{z_3}{z_4}\right) \frac{z_r}{z_s + z_r} \left(-\frac{z_1}{z_2}\right) q_1 + \left(-\frac{z_3}{z_4}\right) \frac{z_s}{z_s + z_r} q_2 \quad (18)$$

$$p_D = \left(-\frac{z_3}{z_4}\right) \frac{z_s + z_r}{z_r} \left(-\frac{z_1}{z_2}\right) q_1 + \left(-\frac{z_3}{z_4}\right) \left(-\frac{z_s}{z_r}\right) q_2 \quad (19)$$

It could be observed from Equation (16) to Equation (19) that the planetary gears only serve the function of combining q_1 and q_2 . Even the planetary gears are identical for all the outputs, specific coefficients for q_1 and q_2 could still be realized by the z_1/z_2 and z_3/z_4 ratios. In order to reduce the fabrication cost, all the planetary gears were hence made identical. What's more, the postural synergies (\mathbf{u}_1 and \mathbf{u}_2) from Table 2 are generated from the SVD of the pose matrix. $\|\mathbf{u}_1\| = \|\mathbf{u}_2\| = 1$. Equation (5) still holds if the \mathbf{u}_1 and \mathbf{u}_2 values are increase κ times while the q_1 and q_2 values are reduced κ times at the same time. The new values of \mathbf{u}_1 and \mathbf{u}_2 are denoted as \mathbf{u}'_1 and \mathbf{u}'_2 in Table 3, which facilitates the design of the gear ratios.

The process of designing the gear system can be summarized as follows:

- (1) Assume the coefficient κ to obtain the \mathbf{u}'_1 and \mathbf{u}'_2 values as the design goal.
- (2) Assume the teeth numbers for the planetary gears, namely, the z_s and z_r values.
- (3) Select a proper configuration from Figure 10 to design the gear teeth for the seven non-coupled joints (e.g. the T_{rot} , the T_{abd} , the T_{mcp} , the I_{mcp} , the M_{mcp} , the R_{mcp} , and the L_{mcp} joints). The configuration selection criterion is according to the ratio of the corresponding elements in \mathbf{u}_1 and \mathbf{u}_2 : select configuration A for $-1 < \eta = u_1/u_2 < 0$, configuration B for

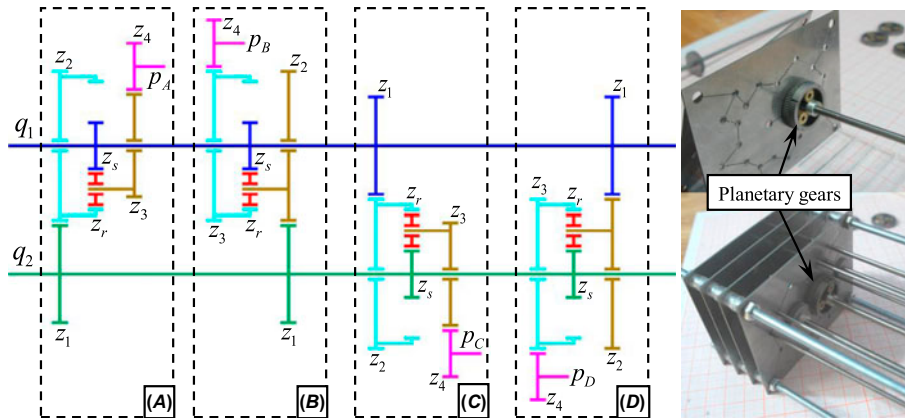


Figure 10. Design of the planetary gear transmission unit and the assembly.

Table 3. The adjusted postural synergies and the realized synergies.

Joints	Adjusted synergies		Realized synergies		Config	Teeth number					
	u'_1	u'_2	u''_1	u''_2		z_1	z_2	z_s	z_r	z_3	z_4
T_{rot}	-0.1232	0.0590	-0.1228	0.0595	C	52	68	20	54	72	-18
T_{mcp}	-0.0406	-0.0514	-0.0395	-0.0532	B	32	88			83	-25
T_{ip}	-0.0379	-0.0586	-0.0401	-0.0540	B	32	88			87	-13
T_{abd}	-0.0494	-0.0437	-0.0504	-0.0428	D	29	91			67	-29
I_{mcp}	0.0848	-0.1644	0.0852	-0.1644	A	50	70			82	-13
M_{mcp}	0.1403	0.0303	0.1398	0.0289	D	68	52			39	25
R_{mcp}	0.1105	0.1257	0.1111	0.1251	B	28	92			84	14
L_{mcp}	0.0376	-0.0631	0.0375	-0.0629	A	46	74			61	-22
I_{pip}	0.0031	0.0161	0.0031	0.0161	A	46	74			85	-13
M_{pip}	-0.0024	-0.0266	-0.0031	-0.0289		82					-30
R_{pip}	-0.0047	0.0207	-0.0037	0.0194	B	32	88	20	54	87	15
L_{pip}	-0.0322	0.0352	-0.0323	0.0347	A	80	40			22	-57
I_{abd}	0.0063	0.0190	0.0	0.0102		70					-38
R_{abd}	-0.0125	-0.0038	0.0	0.0102							
L_{abd}	-0.0047	0.0178	0.0	0.0204							

$0 < \eta < 1$, configuration C for $\eta < -1$, and configuration D for $\eta > 1$.

- (4) Select a proper configuration from Figure 10 to design the gear teeth for the five coupled joints (e.g. the T_{ip} , the I_{pip} , the M_{pip} , the R_{pip} , and the L_{pip} joints) based on the design results in Step (3).
- (5) Step (3) or (4) should be terminated and go back to Step (2) or even Step (1) if the design results lead to a synergy value with an error bigger than 5%.

Please note that the 5% accuracy above was determined based on a trade-off between the accuracy and the overall size of the transmission unit. Since the synergy is realized by discrete gear ratios, the improvement on the accuracy will lead to an increase in the gear teeth and a bigger transmission unit. At the 5% accuracy, both the accuracy and the overall size are considered acceptable.

A design example for the T_{mcp} joint is as follows. An initial coefficient $\kappa = 0.25$ is selected. The synergy values for the T_{mcp} joint become -0.0406 and -0.0514 from the original values of -0.16 and -0.21 from Table 2. The ratio is 0.79 so configuration B is selected. Then the overall transmission is governed by Equation (20), which is obtained by substituting Equation (9) into Equation (17). The design results are listed in the second row of Table 3. The realized synergy values (in the column of u''_1 and u''_2) are shown as -0.0395 and -0.0532 .

$$j_{T_{mcp}} = \frac{9}{280} \left(-\frac{z_3}{z_4} \right) \left(-\frac{z_s}{z_r} \right) q_1 + \frac{9}{280} \left(-\frac{z_3}{z_4} \right) \frac{z_s + z_r}{z_r} \left(-\frac{z_1}{z_2} \right) q_2 \quad (20)$$

For the coupled joint such as the T_{ip} joint, the first row of Equation (21) is the design goal, which is the dependence of the T_{ip} joint angle on q_1 and q_2 inputs. The second row of Equation (21) is obtained by substituting Equation (20) into Equation (10), which is the actual realization. In order to properly select a proper configuration from Figure 10 for the $p_{T_{ip}}$ output, the design-goal synergy values of the T_{ip} joint ($u'_{1|T_{ip}} = -0.0379$ and $u'_{2|T_{ip}} = -0.0586$ in the 3rd row in Table 3) should be added to the realized synergy values of the T_{mcp} joint ($u''_{1|T_{mcp}} = -0.0395$ and $u''_{2|T_{mcp}} = -0.0532$). Then the ratio is $\eta = (-0.0379 - 0.0395) / (-0.0586 - 0.0532) = 0.69$ and configuration B should be selected. The overall transmission is governed by Equation (22). The design results are listed in the third row of Table 3 with the realized synergy values shown as -0.0401 and -0.0540 .

$$j_{T_{ip}} = u'_{1|T_{ip}} q_1 + u'_{2|T_{ip}} q_2 \quad \leftrightarrow \quad j_{T_{ip}} = \frac{9}{280} p_{T_{ip}} - (u''_{1|T_{mcp}} q_1 + u''_{2|T_{mcp}} q_2) \quad (21)$$

$$j_{T_{ip}} = \left(\frac{9}{280} \left(-\frac{z_3}{z_4} \right) \left(-\frac{z_s}{z_r} \right) - u''_{1|T_{mcp}} \right) q_1 + \left(\frac{9}{280} \left(-\frac{z_3}{z_4} \right) \frac{z_s + z_r}{z_r} \left(-\frac{z_1}{z_2} \right) - u''_{2|T_{mcp}} \right) q_2 \quad (22)$$

The rest of the planetary gears could be designed similarly. The design results are summarized in Table 3.

Particular attention should be directed to the coupled M_{pip} joint. Similarly to the T_{ip} joint, in order to properly select a proper configuration of the planetary gear, the design-goal synergy values of the M_{pip} joint ($u'_{1|M_{pip}} = -0.0024$ and $u'_{2|M_{pip}} = -0.0266$ in Table 3)

should be added to the realized synergy values of the M_{mcp} joint ($u''_{1|M_{mcp}} = 0.1398$ and $u''_{2|M_{mcp}} = 0.0289$). Then the ratio is about $\eta = (-0.0024 + 0.1398)/(-0.0266 + 0.0289) = 59.74$. Although it falls into the ratio range for configuration D, it could be considered the output primarily depends on q_1 , since $\eta = u_1/u_2 \gg 1$. Hence, instead of using another set of planetary gears, two meshed spur gears are used (z_1 as the input and z_4 as the output in the M_{pip} row of Table 3). The overall transmission is governed by Equation (23), which is obtained by substituting the synergy results for the M_{mcp} joint into Equation (12). The realized synergy values are -0.0031 and -0.0289 . This realized synergy value $u''_{2|M_{pip}} = -0.0289$ has an error more than 5%, which seems to violate Step (5) of the design procedure. However, the error could have been diminished if one more set of planetary gears had been used. In a future development, the designer could decide on his/her own to tolerate the error or to add one more set of planetary gears.

$$\begin{aligned} j_{M_{pip}} &= \frac{1}{20} p_{M_{pip}} - j_{M_{mcp}} \\ &= \frac{1}{20} \left(-\frac{z_1}{z_4} \right) q_1 - (u''_{1|M_{mcp}} q_1 + u''_{2|M_{mcp}} q_2) \\ &= \left(\frac{1}{20} \left(-\frac{z_1}{z_4} \right) - u''_{1|M_{mcp}} \right) q_1 - u''_{2|M_{mcp}} q_2 \end{aligned} \quad (23)$$

For the coupled I_{abd} , the R_{abd} and the L_{abd} joints, the design-goal synergy values are considered with lower accuracy because when the dummy hands were manually posed, unnecessary abduction/adduction motions could have been introduced. The three joints were made coupled and only a pair of spur gears is used for the transmission. The gear ratio was accepted since the introduced errors are less than 2.0° . The overall transmissions for the I_{abd} , the R_{abd} , and the L_{abd} joints are in Equation (24) to Equation (26), derived from Equation (13) to Equation (15) with z_1 as the input and z_4 as the output gears.

$$j_{I_{abd}} = 0.00556 p_{abd} = 0.00556 \left(-\frac{z_1}{z_4} \right) q_2 \quad (24)$$

$$j_{R_{abd}} = 0.00556 p_{abd} = 0.00556 \left(-\frac{z_1}{z_4} \right) q_2 \quad (25)$$

$$j_{L_{abd}} = 0.0111 p_{abd} = 0.0111 \left(-\frac{z_1}{z_4} \right) q_2 \quad (26)$$

It could be seen from Figure 10 that z_1 is always meshed with z_2 . There is an implicit constraint that the

sum of z_1 and z_2 shall be a constant so that two straight shafts could be used. In the current design, $z_1 + z_2 = 120$. The gear z_3 is always meshed to z_4 for the output. A negative value for z_4 means an idler was used to change the direction of the output. Different sums of z_3 and z_4 actually helped the distribution of the output shafts. The outputs are joined to the flexible shafts to drive the anthropomorphic hand.

All the gears in the transmission system have a module of 0.3. They were manufactured using wire EDM. The assembling process could be viewed in Figure 10.

4. Experimental characterization

With the anthropomorphic hand and the transmission unit built, four sets of experiments were carried out to examine the characteristics of the hand.

4.1. Quantification of the transmission errors

Two synergy inputs (q_1 and q_2) are scaled and combined to generate 13 synergy outputs ($p_{T_{rot}}$, $p_{T_{abd}}$, $p_{T_{mcp}}$, and so on) through the transmission unit. The first set of experiments was conducted to quantify the transmission errors from the planetary gear system.

The experimental setup is shown in Figure 11(a). Two Maxon DC servomotors were controlled by a Matlab xPC Target to drive the two synergy inputs. Motion control cards included the D/A card PCL-727 from the AdvanTech Inc and the counter card CNT32-8M from the Contec Inc. The synergy outputs were examined one by one using another encoder. The synergy output p depends on the two inputs as in Equation (27), where \tilde{u}_1 and \tilde{u}_2 are coefficients of the planetary gears and they have forms as the coefficients in front of q_1 and q_2 as in Equation (16) to Equation (19). Specific values of \tilde{u}_1 and

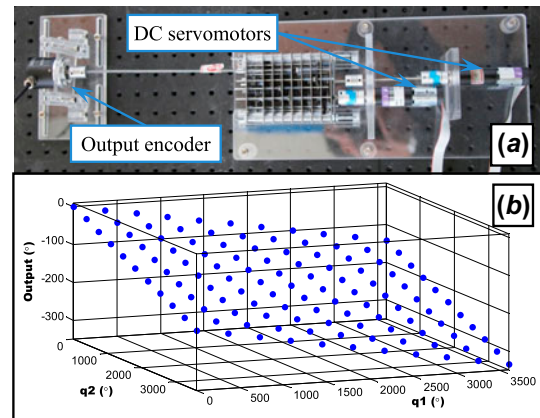


Figure 11. Experiment for the transmission error quantification: (a) the setup and (b) the a representative result for the T_{mcp} joint.

\tilde{u}_2 can be calculated using the teeth numbers and the configuration type from Table 3.

$$p = \tilde{u}_1 q_1 + \tilde{u}_2 q_2 \quad (27)$$

Readings from the encoder for one synergy output was plotted with respect to the two synergy inputs. A representative plot for the T_{mcp} joint is shown in Figure 11(b) with the blue dots as the measured rotary outputs. The transmission errors could be calculated as the differences between the readings and the desired values. The experimental results showed that these errors have an average about 8° to 17° . These errors primarily come from the backlash of the customized gear system. Since many of the outputs will be connected to a worm and gear with a reduction ratio of 20:1. The errors on the hand joints would be smaller than one degree if the backlashes in the hand are not included. The transmission accuracy of the planetary gear system was considered acceptable.

4.2. Force capabilities of the hand fingers

After experimentally verifying the transmission accuracy in Section 4.1, the second sets of the experiments were conducted to examine the force capabilities of the hand fingers.

Two motors as the synergy inputs drive the transmission unit so that 13 outputs drive the anthropomorphic hand. Due to the mechanical synergy design, each output will be determined by the two inputs together. For simplicity, the force capabilities are quantified when the q_1 motor was solely used. Furthermore, when one joint is measured, the flexible shafts of other joints are disconnected.

The experimental setup is shown in Figure 12. Different forces were applied to a finger by hanging weights through two pulleys. A bore array was used to arrange the pulley positions freely so that the applied force was always perpendicular to the corresponding phalange.

For example, forces were applied to the M_{pip} joint as shown in Figure 12 and the force direction was approximately perpendicular to the intermediate phalange of the middle finger. Weights were incrementally increased to 250 grams to stall the motor (Maxon A-max 22 motor with a GP 22A gearhead and MR encoder). Stalling weights for other hand joints range between 210 and 280 g. The miniature worms & gears used in the hand only have an efficiency of 20–30%. The transmission unit also has some friction because the gears were fabricated using wire EDM without grinding or surface treatments. The stalling forces could be increased by improving the manufacturing grades of the components.

The flexible shafts have a rated torsional stiffness of 150 mNm per rad per meter. The torsional deflection is

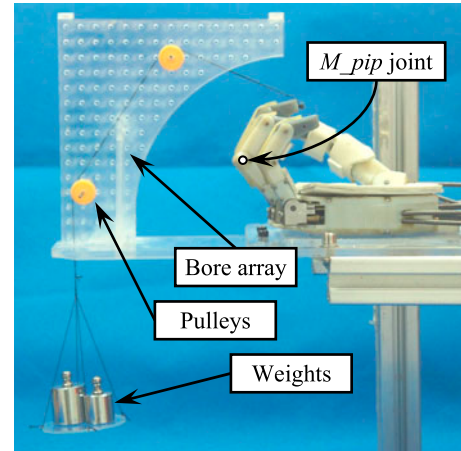


Figure 12. Experimental setup for the loading capability of the fingers.

about 9.55° while lifting a 200 gram weight. This torsional deflection would correspond to a joint angle error of less than 0.5° due to the gear ratio of the worm and gear. Hysteresis of the flexible shafts was not observed other than the torsional deflections.

4.3. Rotate the rehabilitation training balls

The outputs from the transmission unit are connected to the anthropomorphic hand via the flexible shafts so that the hand is actuated by the two synergy inputs. Two motors were commanded to the desired input values to reproduce the intended motion sequence of rotating the two rehabilitation training balls. The synergy inputs (q_1 and q_2) for the corresponding six key poses are now four times of their initial values from Table 2 because a coefficient $\kappa = 0.25$ was used for the transmission unit design.

The hand was firstly posed to the average pose specified by \mathbf{j} . Then the synergy inputs (q_1 and q_2) were commanded for Pose 1 in the motion sequence. Two rehabilitation training balls were placed on the palm and the two synergy inputs were then commanded to the rest five key poses. The reference trajectories of the synergy inputs are generated via spline interpolation. The reference and the actual trajectories are plotted in Figure 13(a). The delay between the reference and the actual trajectories ranges between 50 and 80 ms. The realized six key poses of the hand during the manipulation motion are shown in Figure 13(b). Manipulating the two rehabilitation training balls on the palm in a cyclic manner was successful. The ball manipulation speed was not very high, since a motion cycle is 6 s as shown in Figure 13(a). The balls' dynamics might not play a critical role in the success of their manipulation.

Comparing with the poses in Figure 3, there are discrepancy and errors between the poses of the dummy

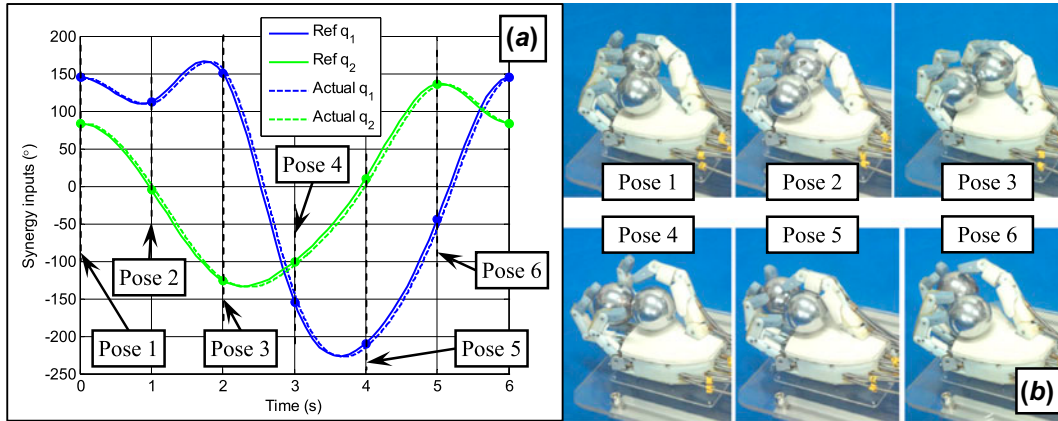


Figure 13. Manipulation of the two training balls: (a) trajectories of the synergy inputs and (b) the six key poses.

hand and that of the anthropomorphic hand. The discrepancies were quantified as follows. Geometrical features were reserved in the fingertip as shown in the inset of Figure 14(a). The optical tracker was used to identify the actual position and orientation of the fingertips. The desired hand poses could be calculated from the realized synergies and the kinematic parameters of the hand. The actual (spherical fingertips) and the desired (cylindrical fingertips) Pose 3 and Pose 5 in the motion sequence are visualized in Figure 14(b) and (c), respectively. The position errors range from 2.7 to 9.1 mm and the orientation errors range from 3.0° to 11.9° . These errors primarily stem from the manufacturing tolerances, assembly errors, and backlashes in the mechanical structures of the anthropomorphic hand and the transmission unit.

Although the ball manipulation task was successful, it is still interesting to further compare the ball manipulation motions performed by the underactuated anthropomorphic hand and by human subjects. The experimental setup is shown in Figure 15(a). Two healthy human subjects were asked to manipulate the training balls and the motions were recorded. In order to make the comparison more consistent, palm positions of the hand and the

human subjects were matched before the manipulation motions.

Frames were extracted from these video clips and were processed. The frames were firstly turned into gray scale and then turned into black-and-white images by setting a proper threshold gray level. The Hugh transformation was applied to these black-and-white images to detect the balls and the centers. Detected features were overlaid back to the images as shown in Figure 15(b) to verify the detections. The detected centers of the balls are plotted in the image coordinates as shown in Figure 15(c). The solid and the dashed lines represent the trajectories of the two balls. The trajectories from the human manipulation motions are overlaid in Figure 15(c) matching the positions of the two black markers as shown in Figure 15(b).

It could be observed from Figure 15(c) that the trajectories are quite different when the balls are manipulated by the underactuated hand and by the human subjects. The trajectory discrepancy in Figure 15(c) can be as big as 25–30 pixels, which is approximately 7.5–9.0 mm. This conversion is based on the ball's actual diameter of 44.5 mm and its diameter of about

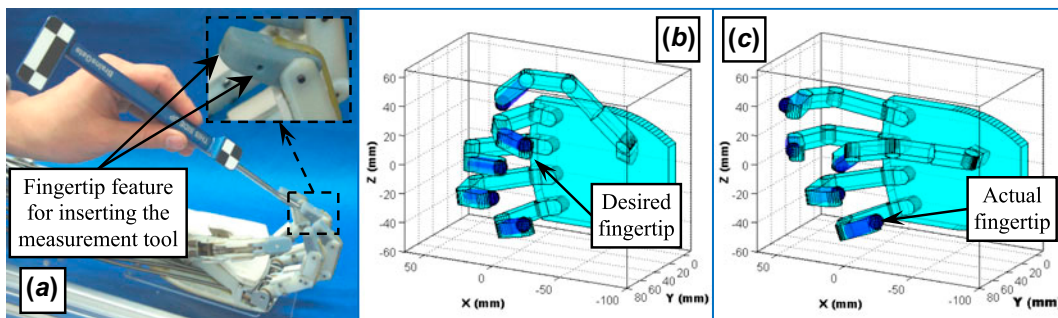


Figure 14. Quantification of the motion discrepancy: (a) experimental setup, the actual and the desired positions and orientations of the fingertips for (b) Pose 3 and (c) Pose 5.

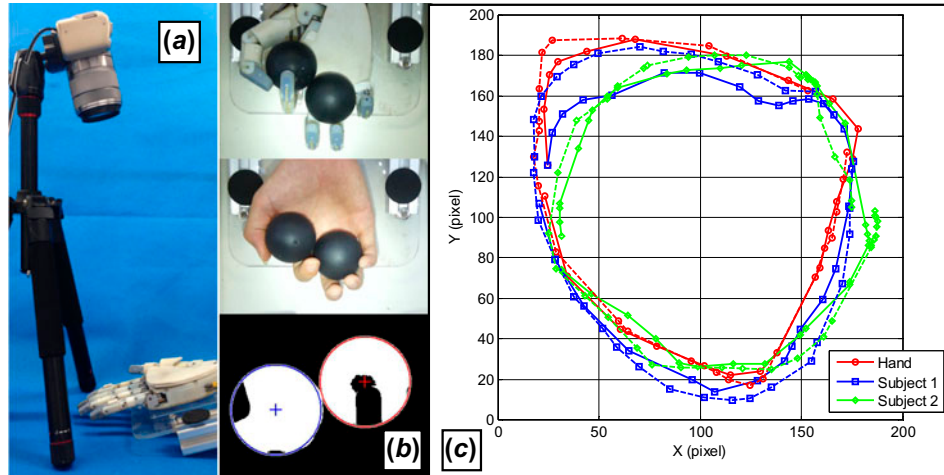


Figure 15. Quantitative comparison of the ball manipulation: (a) experimental setup, (b) video feed analysis, and (c) ball trajectories.

151 pixels in the images. Since the ball trajectories are constrained by the fingers, the discrepancy in the ball trajectories could correspond to the motion discrepancy of the fingers. From the experiments in Figure 14, the position discrepancy between the desired and the actual fingertips of the hand ranges from 2.7 to 9.1 mm. Hence, it is very possible that the ball trajectories by the robotic hand in Figure 15(c) differ from the ball trajectories in Figure 2 when the balls were manipulated by the dummy hand, even though the ball manipulation was achieved successfully.

4.4. Grasping capabilities

CNS switches between different sets of postural synergies for distinct groups of hand motions. It could be considered the synergies from the ball-rotating motions could be quite different from the ones for daily grasping poses. The fourth experimentation explores whether the synergies from the ball-rotating motions could still be used for some grasping tasks.

When the planetary gear transmission unit was used as the mechanical implementation of the postural synergies, the valid actuation zone in Figure 5 shall be updated using the realized synergies (\mathbf{u}''_1 and \mathbf{u}''_2) from Table 3. The updated actuation zone is shown in Figure 16(a).

The synergy inputs (q_1 and q_2) were varied within the allowed actuation zone to check the hand's capabilities in grasping daily life objects. Five representative grasping poses are shown in Figure 16(b.1)–(b.5) with their corresponding q_1 and q_2 values marked in Figure 16(a). An uncommon pose is shown in Figure 16(b.6) with the synergy inputs from the lowest corner of the allowed actuation zone. This pose does not seem to provide a common grasping capability and it is formed due to the postural synergies from the ball-rotating motions. As long as the synergy inputs (q_1 and q_2) can be continuously commanded, all the hand poses can be continuously transformed from one to another.

An exhaustive examination of the grasping capability of the presented design could refer to the milestone work

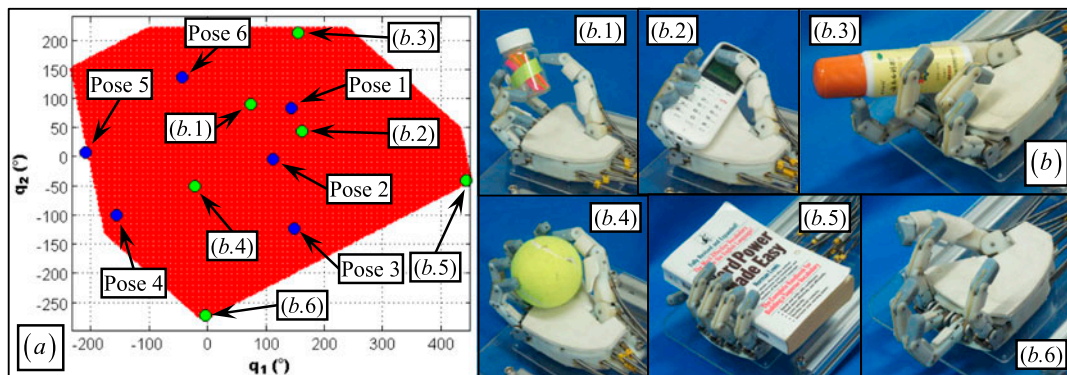


Figure 16. (a) Allowed actuation zone of the two inputs using the realized postural synergies; (b) various grasping poses: (b.1) a small jar, (b.2) a phone, (b.3) a spray, (b.4) a ball, (b.5) a book, and (b.6) an uncommon pose.

[23] where an optimizer checks whether a stable grasp of an arbitrary object could be achieved. An experimental repetition of such a process involves: (i) haptic sensing on the hand fingertips, (ii) an optical system to measure object surface normals, and (iii) a positioner to place the object with respect to the hand correctly. Such a process could be out of the current scope of this paper which intends to study the feasibility of mechanical implementation of postural synergies.

Due to the use of the postural synergies extracted from dissimilar pose patterns (ball manipulation vs. daily grasping poses), the grasping capabilities of the hand are limited. For example, it failed to grasp slim objects (e.g. pens, screw drivers) and broad objects (e.g. CDs, toilet paper rolls) because the required grasping patterns do not appear in the motion sequence of rotating the two training balls. If the synergies had been extracted from various daily grasps, the hand's capabilities in reproducing these poses shall certainly be satisfactory.

5. Conclusions

This paper proposes to implement the postural synergies mechanically and presents a complete process of constructing an underactuated anthropomorphic hand, elaborating synergy synthesis, hand design, mechanical synergy implementation, and experimental characterization.

A specific motion paradigm is selected as the manipulation of two rehabilitation training balls. By constructing a dummy hand, the postural synergies were extracted conveniently in a cost-effective way. The synthesized synergies were then adjusted to suppress the critical errors which might hinder the reproduction of the desired hand poses.

Referring to the postural synergies and the anthropomorphic hand design, a transmission unit was designed using planetary gears as the mechanical synergy implementation. Two rotation inputs can be scaled, combined, and mapped to 13 rotary outputs to drive the joints of the anthropomorphic hand. Using these two synergy inputs, manipulation of the two training balls was successfully carried out. The results suggest that it is possible to upgrade the motion capabilities of a synergy-driven hand from object grasping to more delicate motions (such as object manipulation).

Further experimentation shows the hand's grasping capabilities are limited, because the implemented synergies were not extracted from a comprehensive set of grasping poses. It can be considered that the hand poses of the manipulation task and comprehensive grasps belong to two distinct sets. The postural synergies extracted from one set will have limited capabilities in reproducing the poses in the other set. If the synergies had been extracted from various daily grasps, the hand's capabilities in reproducing these poses shall certainly be satisfactory.

Using smaller gears and optimizing the arrangement of the planetary gear sets, it is very possible to apply the anthropomorphic hand as prosthesis. The results presented here suggest it might be quite promising to construct a low cost yet versatile prosthetic hand with mechanically implemented postural synergies. In such a future development, some improvements could be considered, such as integrating joint compliance to ensure a smoother manipulation or to form grasps with more stable force closures.

Funding

This work was supported in part by the National Program on Key Basic Research Projects [grant number 2011CB013300], in part by the Science and Technology Commission of Shanghai Municipality [grant number 13430721600], and in part by the National Natural Science Foundation of China [grant number 51375296].

Notes on contributors



Kai Xu received the BE and MS degrees from the Department of Precision Instruments and Mechanology, Tsinghua University, Beijing, China, in 2001 and 2004, respectively, and the PhD degree (with distinction) from the Department of Mechanical Engineering, Columbia University, New York, NY, in 2009. Since 2010, he has been with the University of Michigan – Shanghai Jiao Tong University Joint Institute, Shanghai Jiao Tong University, Shanghai, China, where he is currently an assistant professor and the director of the Robotics Innovation and Intervention Laboratory. His research interests include surgical robots, exoskeletons, humanoid robots, prosthetic hands, special industrial robots, and continuum mechanisms.



Huan Liu received the BS degree from the School of Mechanical Engineering, Huazhong Agricultural University, Wuhan, China, in 2008, and the MS degree from the School of Power and Mechanical Engineering, Wuhan University, Wuhan, China, in 2010. He is currently pursuing his PhD degree in the University of Michigan – Shanghai Jiao Tong University Joint Institute, Shanghai Jiao Tong University, Shanghai, China. His research interests include prosthetic hands and biomechanics.



Yuheng Du received the BS degree from the University of Michigan – Shanghai Jiao Tong University Joint Institute, Shanghai Jiao Tong University, Shanghai, China in 2013. He is currently pursuing his MS degree in the same institute.



Xiangyang Zhu received the BS degree from the Department of Automatic Control Engineering, Nanjing Institute of Technology, Nanjing, China, in 1985, the MPhil degree in instrumentation engineering and the PhD degree in automatic control engineering, both from Southeast University, Nanjing, China, in 1989 and 1992, respectively. From 1993 to 1994, he was a post-doctoral research fellow with Huazhong

University of Science and Technology, Wuhan, China. He joined the Department of Mechanical Engineering as an associate professor, Southeast University, in 1995. Since June 2002, he has been with the School of Mechanical Engineering, Shanghai Jiao Tong University, Shanghai, China, where he is currently a Changjiang chair professor and the director of the Robotics Institute. His current research interests include robotic manipulation planning, human-machine interfacing, and bio-mechatronics. Dr Zhu received the National Science Fund for Distinguished Young Scholars in 2005.

References

- [1] Bicchi A. Hands for dexterous manipulation and robust grasping: a difficult road toward simplicity. *IEEE Trans. Robot. Autom.* 2000;16:652–662.
- [2] Gazeau JP, Zehloul S, Arsicault M, et al. The LMS hand: force and position controls in the aim of the fine manipulation of objects. In: *Proceedings of the IEEE International Conference on Robotics and Automation*. Seoul; 2001 May 21–26.
- [3] Liu H, Meusel P, Seitz N, Willberg B, Hirzinger G, Jin MH, Liu YW, Wei R, Xie ZW. The modular multisensory DLR-HIT-Hand. *Mech. Mach. Theory.* 2007;42:612–625.
- [4] Grebenstein M, Chalon M, Friedl W, Haddadin S, Wimbock T, Hirzinger G, Siegwart R. The hand of the DLR hand arm system: Designed for interaction. *Int. J. Robot. Res.* 2012;31:1531–1555.
- [5] Napier JR. The prehensile movements of the human hand. *J. Bone Joint Surg.* 1956;38:902–913.
- [6] Elliott JM, Connolly KJ. A classification of manipulative hand movements. *Dev. Med. Child Neurol.* 1984;26:283–296.
- [7] Cutkosky MR. On grasp choice, grasp models, and the design of hands for manufacturing tasks. *IEEE Trans. Robot. Autom.* 1989;5:269–279.
- [8] Carrozza MC, Cappiello G, Micera S, Edin BB, Beccai L, Cipriani C. Design of a cybernetic hand for perception and action. *Biol. Cybern.* 2006;95:629–644.
- [9] Gosselin C, Pelletier F, Laliberté T. An anthropomorphic underactuated robotic hand with 15 Dofs and a single actuator. In: *Proceedings of the IEEE International Conference on Robotics and Automation*. Pasadena (CA); 2008 May 19–23.
- [10] Dalley SA, Wiste TE, Withrow TJ, Goldfarb M. Design of a multifunctional anthropomorphic prosthetic hand with extrinsic actuation. *IEEE/ASME Trans. Mechatron.* 2009;14:699–706.
- [11] Cipriani C, Controzzi M, Carrozza MC. Objectives, criteria and methods for the design of the SmartHand transradial prosthesis. *Robotica.* 2010;28:919–927.
- [12] Feix T, Pawlik R, Schmiedmayer H-B, Romero J, Kragić D. A comprehensive grasp taxonomy. In: *Robotics, Science and Systems: Workshop on Understanding the Human Hand for Advancing Robotic Manipulation*. Seattle (WA); 2009.
- [13] Zheng JZ, De La Rosa S, Dollar AM. An investigation of grasp type and frequency in daily household and machine shop tasks. In: *Proceedings of the IEEE International Conference on Robotics and Automation*. Shanghai, China; 2011 May 9–13.
- [14] Bernstein N. The problem of the interrelation of coordination and localization. *Arch. Biol. Sci.* 1935;38:1–34.
- [15] Santello M, Flanders M, Soechting JF. Postural hand synergies for tool use. *J. Neurosci.* 1998;18:10105–10115.
- [16] Weiss EJ, Flanders M. Muscular and postural synergies of the human hand. *J. Neurophysiol.* 2004;92:523–535.
- [17] Wimböck T, Jahn B, Hirzinger G. Synergy level impedance control for multifingered hands. In: *Proceedings of the IEEE/RSJ International Conference on Intelligent Robots and Systems*. San Francisco (CA); 2011 Sept 25–30.
- [18] Rosell J, Suárez R, Rosales C, Pérez A. Autonomous motion planning of a hand-arm robotic system based on captured human-like hand postures. *Auton. Robot.* 2011;31:87–102.
- [19] Ficuciello F, Palli G, Melchiorri C, Siciliano B. Experimental evaluation of postural synergies during reach to grasp with the UB Hand IV. In: *Proceedings of the IEEE/RSJ International Conference on Intelligent Robots and Systems*. San Francisco (CA); 2011 Sept 25–30.
- [20] Rombokas E, Malhotra M, Matsuoka Y. Task-specific demonstration and practiced synergies for writing with the ACT hand. In: *Proceedings of the IEEE International Conference on Robotics and Automation*. Shanghai, China; 2011 May 9–13.
- [21] Zhang A, Malhotra M, Matsuoka Y. Musical piano performance by the ACT hand. In: *Proceedings of the IEEE/RSJ International Conference on Intelligent Robots and Systems*. Shanghai, China; 2011 May 9–13.
- [22] Brown CY, Asada HH. Inter-finger coordination and postural synergies in robot hands via mechanical implementation of principal components analysis. In: *Proceedings of the IEEE/RSJ International Conference on Intelligent Robots and Systems*. San Diego (CA); 2007 Oct 29–Nov 2.
- [23] Ciocarlie MT, Allen PK. Hand posture subspaces for dexterous robotic grasping. *Int. J. Robotics Res.* 2009;28:851–867.
- [24] Gioioso G, Salvietti G, Malvezzi M, Prattichizzo D. Mapping synergies from human to robotic hands with dissimilar kinematics: an approach in the object domain. *IEEE Trans. Robotics.* 2013;29:825–837.
- [25] Xu K, Zhao J, Du Y, Sheng X, Zhu X. Design and postural synergy synthesis of a prosthetic hand for a manipulation task. In: *Proceedings of the IEEE/ASME International Conference on Advanced Intelligent Mechatronics*. Wollongong, Australia; 2013 July 9–12.
- [26] Kawasaki H, Komatsu T, Uchiyama K. Dexterous anthropomorphic robot hand with distributed tactile sensor: Gifu hand II. *IEEE/ASME Trans. Mechatron.* 2002;7:296–303.
- [27] Huang H, Jiang L, Liu Y, Hou L, Cai H, Liu H. The mechanical design and experiments of HIT/DLR prosthetic hand. In: *Proceedings of IEEE International Conference on Robotics and Biomimetics*. Kunming, China; 2006 Dec 17–20.